

Dr. Arnaud Mignan  
Institute of Geophysics,  
Swiss Federal Institute of Technology, Zürich  
NO H66, Sonneggstrasse 5  
CH-8092 Zürich  
[arnaud.mignan@sed.ethz.ch](mailto:arnaud.mignan@sed.ethz.ch)

22 February 2018

Dear Editor Ilya Zaliapin,

Please find below my answers to your comments, [highlighted in blue](#). I agree that the Solid Seismicity Postulate remains to be verified, so the text was changed to clarify this important point. The only point where I disagree is to discard the term “theory”. As I explain below, what is proposed can be defined as a theory. I hope that this reply answers to all of your remaining concerns.

Sincerely,

Arnaud Mignan

### **Editor’s comments**

#### Comments to the Author:

The revised paper shows a significant improvement in terms of clarity and justification of the main statements. I find that most of the technical comments raised by the reviewers were addressed in this revision. At the same time, there remain several conceptual issues that are being debated by the author. Resolving these issues (mainly, by revising the current text and conclusions) would make the paper acceptable to publication in NPG.

One of the main concerns is that the SSP, the main methodological tool of the work, has not been shown to be a physically justified principle that drives the observed seismicity. Specifically, the SSP seems to be a practical toy model that can be appropriately ramified (e.g., by adding noise, like in Fig. 4) to look consistent with the data. This might be not surprising though: the activity (suitably defined) of aftershocks generally decays away from a mainshock, so a model formulated in terms of decay (continuous or step-like) could be made consistent with data. This observation alone is insufficient to prove the validity of SSP. Nevertheless, the paper claims that the SSP has been validated (l. 16) and the SSP is a “proper approach” (l. 367) that can explain “most empirical laws observed in seismicity” (l. 356). These claims are unsupported by the analysis presented in the work; I think such claims can distract a reader and harm a potential impact of the work. A possible resolution would be to explicitly introduce SSP as an assumption and illustrate how it can be used to make inference regarding the productivity law. Such analysis might be interesting from various points of view and can stimulate further research. The work nicely illustrates how a basic assumption can be transformed into testable statements

regarding the main laws of seismicity; however an attempt to claim that such an assumption is an actual law of seismicity might be premature.

I consider the suggested revisions as minor. However, if the author insists on physical validity of the SSP as a new paradigm in understanding seismicity, a substantial further research and justification will be required.

I modified the text accordingly. The term “*validated*” was replaced everywhere by “*tested*” (lines 17, 106, 186). I also changed “*suggests that the SSP is a proper approach*” to “*shows that the SSP is consistent with large aftershock observations once uniform noise is added to the stress field*” (line 361) and that other types of noise have yet to be tested (line 362). It was already indicated in the same paragraph that the SSP remains to be proven and is “*so far a rather convenient and pragmatic assumption*” (line 358). I added that “*This result alone is however insufficient to prove the validity of the SSP*” (line 217) and finally deleted the sentence: “*most empirical laws observed in seismicity populations can be explained by...*”.

I list other comments below:

It is worth adding a brief summary and discussion of the findings by Hainzl et al. (2010). Their results seem important for understanding the motivation and some of the results of this work.

I added a brief description of the Hainzl et al. (2010) approach and interpretation lines 175-180.

I. 11: parameter K needs a better definition, e.g. “K is the number of aftershocks triggered by a given mainshock of magnitude M “

done.

I. 14: “Solid Seismicity Postulate” (please insert Postulate)

done.

II. 25-28: Please rewrite the sentence, possibly splitting it into two: one regarding the estimations and the other on the necessity to prove the existence of the kink.

I split the sentence in two, now clearly separating the part on the kink and the part on parameter estimation.

I. 31: explain “most robust”

I replaced “*most robust*” by “*one of the most studied*”

II. 32-33: explain what empirical laws are mentioned here

I added “*such as the Modified Omori Law*” for the temporal one. However there is no name available for the spatial law. The productivity law is defined as Utsu law in the next sentence.

I. 45, Eq(2): Define N and A

done.

II. 65: “Solid Seismicity Postulate” (add Postulate)

done.

I. 71: Revise the subsection title (sounds vague at the moment)

Now changed to “Demonstration of the productivity law by geometric operations”

I. 72: “a geometrical theory of seismicity” does not seem justified. Is it possible to merely formulate the postulate, without calling it a “theory”?

I would prefer to keep the term “theory”. A theory is an explanation that can be repeatedly tested, which is here possible as all parameters are clearly described in algebraic equations. Each seismicity patterns is explicitly categorized into background, quiescence and activation based on a spatial event density definition. On Wikipedia, we read “the strength of a scientific theory is related to the diversity of phenomena it can explain and its simplicity”. The proposed theory can describe aftershock productivity, foreshocks (GRL2012) and induced seismicity (NPG2016) solely based on 2 parameters. It has yet to be fully tested to become an established theory or to be rejected, but it is a theory nonetheless. The idea behind the SSP is new and cannot be related to any existing theory of seismicity. The introduced parameters are also new and not related to any other existing seismicity framework. It also represents an abstract concept that generalizes the definition of seismicity patterns in space and time. Solid Seismicity is also not a model but different models can be developed from it, eg an aftershock production model (this paper), a precursory seismicity model or an induced seismicity model (previous papers). I hope that you can agree with this definition.

I. 75: “strictly categorized” needs to be explained

Now defined lines 96-98 as a “sort of hard labelling”. Any seismicity population is either in one of the 3 classes defined in the SSP and no other.

I. 79, Eq. (5): Please define sigma and delta (explanation + units), and “background stress amplitude range”.

done.

I. 92: Please define r and explain the equation.

done.

I. 113, Eq. (7): the comma must appear after the Eq. in line 113, not in line 114.

corrected.

I. 120: “rupture surface area” (add area)

added.

I. 163: Please explain “step-like spatial behavior”. Does this refer to the spatial density of aftershocks?

this is correct, now clarified.

I. 173: “discredited” in this context sounds as too strong of a term. Can you revise?

I changed “*discredited*” to “*questioned*”.

I. 244: Why “Poisson process”?

Now explained, as “*representing the stochasticity of the count  $K$  of aftershocks produced by a mainshock at any given time.*”

I. 351: Please justify “physical”. Eq. (12) is a consequence of an ad-hoc SS postulate; its connection to physical principles has not been established.

I removed “*physical*”. It was meant to refer to parameters based on physical properties, such as stress or event count.

I. 355-357: I do not find this conclusion justified by the presented analysis (see above).

This sentence has been removed.

II. 365-367: The ability to reproduce the scaling parameter  $q$  should be critically assessed against the number of assumptions and parameters involved in this estimation.

I clarified that  $q$  was retrieved once a uniform noise was added to the stress field and that “*the impact of other types of noise on  $q$  has yet to be investigated*” (lines 362-371)

Throughout the paper:

Please avoid using consecutive parentheses, like in “(Kanamori and Anderson, 1975) (Fig. 1d).”

Please check punctuation marks (commas, periods) in equations.

Done.

1     **Utsu aftershock productivity law explained from geometric operations on the**  
2                             **permanent static stress field of mainshocks**

3                             Arnaud Mignan\*

4

5     Institute of Geophysics, Swiss Federal Institute of Technology, Zurich

6     *Address:* ETHZ, Institute of Geophysics, NO H66, Sonneggstrasse 5, CH-8092 Zurich

7

8     *Correspondence to:* [arnaud.mignan@sed.ethz.ch](mailto:arnaud.mignan@sed.ethz.ch)

9

10 *Abstract:* The aftershock productivity law is an exponential function of the form  
 11  $K \propto \exp(\alpha M)$  with  $K$  the number of aftershocks triggered by a given mainshock of  
 12 magnitude  $M$  and  $\alpha \approx \ln(10)$  the productivity parameter. This law remains empirical  
 13 in nature although it has also been retrieved in static stress simulations. Here, we  
 14 explain this law based on the Solid Seismicity Postulate (SSP), the basis of a  
 15 geometrical theory of seismicity where seismicity patterns are described by  
 16 mathematical expressions obtained from geometric operations on a permanent static  
 17 stress field. We first test the SSP that relates seismicity density to a static stress step  
 18 function. We show that it yields a power exponent  $q = 1.96 \pm 0.01$  for the power-law  
 19 spatial linear density distribution of aftershocks, once uniform noise is added to the  
 20 static stress field, in agreement with observations. We then recover the exponential  
 21 function of the productivity law with a break in scaling obtained between small and  
 22 large  $M$ , with  $\alpha = 1.5\ln(10)$  and  $\ln(10)$ , respectively, in agreement with results from  
 23 previous static stress simulations. Possible biases of aftershock selection, verified to  
 24 exist in Epidemic-Type Aftershock Sequence (ETAS) simulations, may explain the  
 25 lack of break in scaling observed in seismicity catalogues. The existence of the  
 26 theoretical kink remains however to be proven. Finally, we describe how to estimate  
 27 the Solid Seismicity parameters (activation density  $\delta_+$ , aftershock solid envelope  $r_+$   
 28 and background stress amplitude range  $\Delta\sigma_+$ ) for large  $M$  values.

Arnaud Mignan 22.2.2018 10:38  
 Deleted: ,  
 Arnaud Mignan 22.2.2018 10:38  
 Deleted: the mainshock magnitude,

Arnaud Mignan 22.2.2018 10:17  
 Deleted: validate  
 Arnaud Mignan 22.2.2018 10:39  
 Deleted: Solid Seismicity Postulate

Arnaud Mignan 22.2.2018 10:42  
 Deleted: ing  
 Arnaud Mignan 22.2.2018 10:42  
 Deleted: ,  
 Arnaud Mignan 22.2.2018 10:42  
 Deleted: w  
 Arnaud Mignan 22.2.2018 10:43  
 Deleted: only

### 30 1. Introduction

31 Aftershocks, one of the most studied patterns observed in seismicity, are  
 32 characterized by three empirical laws, which are functions of time, such as the  
 33 Modified Omori law (e.g., Utsu et al., 1995), space (e.g., Richards-Dinger et al., 2010;  
 34 Moradpour et al., 2014), and mainshock magnitude (Utsu, 1970a; b; Ogata, 1988).

Arnaud Mignan 22.2.2018 10:44  
 Deleted: robust

Arnaud Mignan 22.2.2018 15:29  
 Deleted: ; Mignan, 2015

45 The present study focuses on the latter relationship, i.e., the Utsu aftershock  
 46 productivity law, which describes the total number of aftershocks  $K$  produced by a  
 47 mainshock of magnitude  $M$  as

$$48 \quad K(M) = K_0 \exp[\alpha(M - m_0)] \quad (1)$$

49 with  $m_0$  the minimum magnitude cutoff (Utsu, 1970b; Ogata, 1988). This relationship  
 50 was originally proposed by Utsu (1970a; b) by combining two other empirical laws,  
 51 the Gutenberg-Richter relationship (Gutenberg and Richter, 1944) and Båth's law  
 52 (Båth, 1964), respectively:

$$53 \quad \begin{cases} N(\geq m) = A \exp[-\beta(m - m_0)] \\ N(\geq M - \Delta m_B) = 1 \end{cases} \quad (2)$$

54 | with  $N$  the number of events above magnitude  $m$ ,  $A$  a seismic activity constant,  $\beta$  the  
 55 magnitude size ratio (or  $b = \beta/\ln(10)$  in base-10 logarithmic scale) and  $\Delta m_B$  the  
 56 magnitude difference between the mainshock and its largest aftershock, such that

$$57 \quad K(M) = N(\geq m_0|M) = \exp(-\beta\Delta m_B) \exp[\beta(M - m_0)] \quad (3)$$

58 with  $K_0 = \exp(-\beta\Delta m_B)$  and  $\alpha \equiv \beta$ . Eq. (3) was only implicit in Utsu (1970a) and  
 59 not exploited in Utsu (1970b) where  $K_0$  was fitted independently of the value taken by  
 60 Båth's parameter  $\Delta m_B$ . The  $\alpha$ -value was in turn decoupled from the  $\beta$ -value in later  
 61 studies (e.g., Seif et al. (2017) and references therein).

62 Although it seems obvious that Eq. (1) can be explained geometrically if the  
 63 volume of the aftershock zone is correlated to the mainshock surface area  $S$  with

$$64 \quad S(M) = 10^{M-4} = \exp[\ln(10)(M - 4)] \quad (4)$$

65 (Kanamori and Anderson, 1975; Yamanaka and Shimazaki, 1990; Helmstetter, 2003),  
 66 there is so far no analytical, physical expression of Eq. (1) available. Although Hainzl  
 67 et al. (2010) retrieved the exponential behavior in numerical simulations where  
 68 aftershocks were produced by the permanent static stress field of mainshocks of

69 different magnitudes, it remains unclear how  $K_0$  and  $\alpha$  relate to the underlying  
70 physical parameters.

71 The aim of the present article is to explain the Utsu aftershock productivity  
72 equation (Eq. 1) by applying a geometrical theory of seismicity (based on the Solid  
73 Seismicity Postulate, SSP), which has already been shown to effectively explain other  
74 empirical laws of both natural and induced seismicity from simple geometric  
75 operations on a permanent static stress field (Mignan, 2012; 2016a). The theory is  
76 applied here for the first time to the case of aftershocks.

77

## 78 2. Physical Expression of the Aftershock Productivity Law

### 79 2.1. Demonstration of the productivity law by geometric operations

80 “Solid Seismicity”, a geometrical theory of seismicity, is based on the  
81 following Postulate (Mignan et al., 2007; Mignan, 2008, 2012; 2016a):

82

83 **Solid Seismicity Postulate (SSP):** *Seismicity can be strictly categorized*  
84 *into three regimes of constant spatiotemporal densities  $\delta$  – background*  
85  *$\delta_0$ , quiescence  $\delta_-$  and activation  $\delta_+$  (with  $\delta_- \ll \delta_0 \ll \delta_+$ ) - occurring*  
86 *respective to the static stress step function:*

$$87 \delta(\sigma) = \begin{cases} \delta_- & , \sigma < -\Delta\sigma_* \\ \delta_0 & , \sigma \leq |\pm\Delta\sigma_*| \\ \delta_+ & , \sigma > \Delta\sigma_* \end{cases} \quad (5)$$

88 *with  $\sigma$  the static stress [bar],  $\Delta\sigma_*$  the background stress amplitude range*  
89 *[bar], a stress threshold value separating two seismicity regimes, and  $\delta$*   
90 *the spatial density of events [events/km<sup>3</sup>] per regime.*

91

Arnaud Mignan 22.2.2018 10:52

Deleted: or

Arnaud Mignan 22.2.2018 10:52

Deleted: “

Arnaud Mignan 22.2.2018 10:52

Deleted: ”

Arnaud Mignan 22.2.2018 10:56

Deleted: by Solid Seismicity



96 We mean by “strictly categorized” that any seismicity population is either part of the  
 97 background, quiescence or activation regime (or class), with no other regime/class  
 98 possible (i.e., a sort of hard labelling). Based on this Postulate, Mignan (2012)  
 99 demonstrated the power-law behavior of precursory seismicity in agreement with the  
 100 observed time-to-failure equation (Varnes, 1989), while Mignan (2016a)  
 101 demonstrated both the observed parabolic spatiotemporal front and the linear  
 102 relationship with injection-flow-rate of induced seismicity (Shapiro and Dinske,  
 103 2009). It remains unclear whether the SSP has a physical origin or not. If not, it would  
 104 still represent a reasonable approximation of the linear relationship between event  
 105 production and static stress field in a simple clock-change model (Hainzl et al., 2010;  
 106 Fig. 1a). For the testing of the SSP on, the observed spatial distribution of aftershocks,  
 107 see section 2.2. The power of Eq. (5) is that it allows defining seismicity patterns in  
 108 terms of “solids” described by the spatial envelope  $r_* = r(\sigma = \pm\Delta\sigma_*)$  where  $r$  is the  
 109 distance from the static stress source (e.g., mainshock rupture) and  $r_*$  the distance  $r$  at  
 110 which there is a change of regime (quiescence/background at  $\sigma = -\Delta\sigma_*$  or  
 111 background/activation at  $\sigma = \Delta\sigma_*$ ). The spatiotemporal rate of seismicity is then a  
 112 mathematical expression defined by the density of events  $\delta$  times the volume  
 113 characterized by  $r_*$  (see previous demonstrations in Mignan et al. (2007) and Mignan  
 114 (2011; 2012; 2016a) where simple algebraic expressions were obtained).

115 In the case of aftershocks, we define the static stress field of the mainshock by

$$116 \sigma(r) = -\Delta\sigma_0 \left[ \left( 1 - \frac{c^3}{(r+c)^3} \right)^{-1/2} - 1 \right] \quad (6)$$

117 with  $\Delta\sigma_0 < 0$  the mainshock stress drop,  $c$  the crack radius and  $r$  the distance from the  
 118 crack. Eq (6) is a simplified representation of stress change from slip on a planar  
 119 surface in a homogeneous elastic medium. It takes into account both the square root

Arnaud Mignan 22.2.2018 15:52

Deleted: ) (

Arnaud Mignan 22.2.2018 15:52

Deleted: (

Arnaud Mignan 22.2.2018 15:52

Deleted: f

Arnaud Mignan 22.2.2018 10:17

Deleted: validation

Arnaud Mignan 22.2.2018 15:53

Deleted: from

Arnaud Mignan 22.2.2018 15:52

Deleted: )

126 singularity at crack tip and the  $1/r^3$  falloff at higher distances (Dieterich, 1994; Fig.  
 127 1b). It should be noted that this radial static stress field does not represent the  
 128 geometric complexity of Coulomb stress fields (Fig. 2a). However we are here only  
 129 interested in the general behavior of aftershocks with Eq. (6) retaining the first-order  
 130 characteristics of this field (i.e., on-fault seismicity; Fig. 2b), which corresponds to the  
 131 case where the mainshock relieves most of the regional stresses and aftershocks occur  
 132 on optimally oriented faults. It is also in agreement with observations, most  
 133 aftershocks being located on and around the mainshock fault traces in Southern  
 134 California (Fig. 2c; see section “Observations & Model Fitting”). The occasional  
 135 cases where aftershocks occur off-fault (e.g., Ross et al., 2017) can be explained by  
 136 the mainshock not relieving all of the regional stress (King et al., 1994; Fig. 2d).

137 For  $r_* = r(\sigma = \Delta\sigma_*)$ , Eq. (6) yields the aftershock solid envelope of the form:

$$138 \quad r_*(c) = \left\{ \frac{1}{\left[1 - \left(1 - \frac{\Delta\sigma_*}{\Delta\sigma_0}\right)^{-2}\right]^{1/3}} - 1 \right\} c = Fc, \quad (7)$$

139 function of the crack radius  $c$  and of the ratio between background stress amplitude  
 140 range  $\Delta\sigma_*$  and stress drop  $\Delta\sigma_0$  (Fig. 1c). With  $\Delta\sigma_0$  independent of earthquake size  
 141 (Kanamori and Anderson, 1975; Abercrombie and Leary, 1993) and  $\Delta\sigma_*$  assumed  
 142 constant,  $r_*$  is directly proportional to  $c$  with proportionality constant, or stress factor,  
 143  $F$  (Eq. 7). Geometrical constraints due to the seismogenic layer width  $w_0$  then yield

$$144 \quad c(M) = \begin{cases} \left(\frac{S(M)}{\pi}\right)^{1/2} & , S(M) \leq \pi w_0^2 \\ w_0 & , S(M) > \pi w_0^2 \end{cases} \quad (8)$$

145 with  $S$  the rupture surface [area](#) defined by Eq. (4) and  $c$  becoming an effective crack  
 146 radius (Kanamori and Anderson, 1975; Fig. 1d). Note that the factor of 2 (i.e., using  
 147  $w_0$  instead of  $w_0/2$ ) comes from the free surface effect (e.g., Kanamori and Anderson,  
 148 1975; Shaw and Scholz, 2001).

Arnaud Mignan 22.2.2018 15:55

Deleted: ) (

Arnaud Mignan 22.2.2018 15:56

Deleted: ) (

Arnaud Mignan 22.2.2018 11:43

Deleted: ,

Arnaud Mignan 22.2.2018 15:56

Deleted: ) (

153 The aftershock productivity  $K(M)$  is then the activation density  $\delta_+$  times the  
 154 volume  $V_*(M)$  of the aftershock solid. For the case in which the mainshock relieves  
 155 most of the regional stress, stresses are increased all around the rupture (King et al.,  
 156 1994), which is topologically identical to stresses increasing radially from the rupture  
 157 plane (Fig. 2a-b). It follows that the aftershock solid can be represented by a volume  
 158 of contour  $r_*(M)$  from the rupture plane geometric primitive, i.e., a disk or a  
 159 rectangle, for small and large mainshocks, respectively. This is illustrated in Figure  
 160 3a-b and can be generalized by

$$161 \quad V_*(M) = 2r_*(M)S(M) + \frac{\pi}{2}r_*^2(M)d \quad (9)$$

162 where  $d$  is the distance travelled around the geometric primitive by the geometric  
 163 centroid of the semi-circle of radius  $r_*(M)$  (i.e., Pappus's Centroid Theorem), or

$$164 \quad d = \begin{cases} 2\pi \left( c(M) + \frac{4}{3\pi}r_*(M) \right) & , c(M) + r_*(M) \leq \frac{w_0}{2} \\ 2w_0 & , c(M) + r_*(M) > \frac{w_0}{2} \end{cases} \quad (10)$$

165 For the disk, the volume (Eq. 9) corresponds to the sum of a cylinder of radius  $c(M)$   
 166 and height  $2r_*(M)$  (first term) and of half a torus of major radius  $c(M)$  and minus  
 167 radius  $r_*(M)$  (second term). For the rectangle, the volume is the sum of a cuboid of  
 168 length  $l(M)$  (i.e., rupture length), width  $w_0$  and height  $2r_*(M)$  (first term) and of a  
 169 cylinder of radius  $r_*(M)$  and height  $w_0$  (second term; see red and orange volumes,  
 170 respectively, in Figure 3a-c). Finally inserting Eqs. (7), (8) and (10) into (9), we  
 171 obtain

$$172 \quad K(M) = \delta_+ \begin{cases} \left[ \frac{2F}{\sqrt{\pi}} + F^2\sqrt{\pi} \left( 1 + \frac{4}{3\pi}F \right) \right] S^{3/2}(M) & , S(M) \leq \left( \frac{w_0\sqrt{\pi}}{2(1+F)} \right)^2 \\ \frac{2F}{\sqrt{\pi}} S^{3/2}(M) + F^2 w_0 S(M) & \left( \frac{w_0\sqrt{\pi}}{2(1+F)} \right)^2 < S(M) \leq \pi w_0^2 \\ 2F w_0 S(M) + \pi F^2 w_0^3 & , S(M) > \pi w_0^2 \end{cases}$$

173 (11)

174 which is represented in Figure 3d. Considering the two main regimes only (small  
175 versus large mainshocks) and inserting Eq. (4) into (11), we get

$$176 \quad K(M) = \delta_+ \begin{cases} \left[ \frac{2F}{\sqrt{\pi}} + F^2 \sqrt{\pi} \left( 1 + \frac{4}{3\pi} F \right) \right] \exp \left[ \frac{3 \ln(10)}{2} (M - 4) \right] & , \text{small } M \\ 2Fw_0 \exp[\ln(10)(M - 4)] + \pi F^2 w_0^3 & , \text{large } M \end{cases} \quad (12)$$

177 which is a closed-form expression of the same form as the original Utsu productivity  
178 law (Eq. 1). Note that  $K$  and  $\delta_+$  are both, implicitly, function of the selected minimum  
179 aftershock magnitude threshold  $m_0$ .

180 Here, we predict that the  $\alpha$ -value decreases from  $3 \ln(10)/2 \approx 3.45$  to  $\ln(10) \approx$   
181 2.30 when switching regime from small to large mainshocks (or from 1.5 to 1 in base-  
182 10 logarithmic scale). It should be noted that Hainzl et al. (2010) observed the same  
183 break in scaling in static stress transfer simulations, which corroborates our analytical  
184 findings. [Hainzl et al. \(2010\) simulated aftershocks using the clock-change model](#)  
185 [where events were advanced in time by the static stress change produced by a](#)  
186 [mainshock in a three-dimensional medium. They explained the scaling break](#)  
187 [observed in simulation as a transition from 3D to 2D scaling regime when the](#)  
188 [mainshock rupture dimension approached  \$w\_0\$ , which is compatible with the present](#)  
189 [demonstration](#). For large  $M$ , the scaling is fundamentally the same as in Eq. (4). Since  
190 that relation also explains the slope of the Gutenberg-Richter law (see physical  
191 explanation given by Kanamori and Anderson, 1975), it follows that  $\alpha \equiv \beta$ , which is  
192 also in agreement with the original formulation of Utsu (1970a; b; Eq. 3).

## 194 2.2. [Testing of the SSP on the aftershock spatial distribution](#)

195 The SSP predicts a step-like behavior of [the aftershock spatial density](#) for an  
196 idealized smooth static stress field (Fig. 4a-b), which is in disagreement with real

Arnaud Mignan 22.2.2018 15:59

Deleted: (

Arnaud Mignan 22.2.2018 15:59

Deleted: )

Arnaud Mignan 22.2.2018 15:59

Deleted: ) (

Arnaud Mignan 22.2.2018 10:18

Deleted: Validation

Arnaud Mignan 22.2.2018 10:58

Deleted: Solid Seismicity Postulate

Arnaud Mignan 22.2.2018 16:47

Deleted: spatial

Arnaud Mignan 22.2.2018 11:53

Deleted: s

204 aftershock observations. A number of studies have shown that the spatial linear  
 205 density distribution of aftershocks  $\rho$  is well represented by a power-law, expressed as  
 206  $\rho(r) \propto r^{-q}$  (13)  
 207 with  $r$  the distance from the mainshock and  $q$  the power-law exponent. This parameter  
 208 ranges over  $1.3 \leq q \leq 2.5$  (Felzer and Brodsky, 2006; Lipiello et al., 2009; Marsan and  
 209 Lengliné, 2010; Richards-Dinger et al., 2010; Shearer, 2012; Gu et al., 2013;  
 210 Moradpour et al., 2014; van der Elst and Shaw, 2015). Although Felzer and Brodsky  
 211 (2004) suggested a dynamic stress origin for aftershocks, their results were later on  
 212 **questioned** by Richards-Dinger et al. (2010). Most of the studies cited above suggest  
 213 that the  $q$ -value is explained from a static stress process. **As** for the examples of  
 214 aftershocks shown to be dynamically triggered (e.g., Fan and Shearer, 2016), they are  
 215 too few to alter the aftershock productivity law and too remote to be consistently  
 216 defined as aftershocks in cluster methods.

217 In a more realistic setting, the static stress field must be heterogeneous (due to  
 218 the occurrence of previous events and other potential stress perturbations). We  
 219 therefore simulate the static stress field by adding a uniform random component  
 220 bounded over  $\pm\Delta\sigma_*$  following Mignan (2011) (see also King and Bowman, 2003).  
 221 Note that any deviation above  $\Delta\sigma_*$  would be flattened to  $\Delta\sigma_*$  over time by temporal  
 222 diffusion (so-called “historical ghost static stress field” in Mignan, 2016a). Figure 4c  
 223 shows the resulting stress field and Figure 4d the predicted aftershock spatial density.  
 224 Adding uniform noise blurs the contour of the aftershock solid, switching the  
 225 aftershock spatial density from a step function (Fig. 4b) to a power-law (Fig. 4d). We  
 226 fit Eq. (13) to the simulated data using the Maximum Likelihood Estimation (MLE)  
 227 method with  $r_{min} = r_*$  (Clauset et al., 2009) and find  $q = 1.96 \pm 0.01$ , in agreement with

Arnaud Mignan 22.2.2018 11:54

Deleted: discredited

Arnaud Mignan 22.2.2018 16:00

Deleted: (

Arnaud Mignan 22.2.2018 16:00

Deleted: a

Arnaud Mignan 22.2.2018 16:00

Deleted: )

232 | the aftershock literature. This result alone is however insufficient to prove the validity  
233 | of the SSP.

234

### 235 | 3. Observations & Model Fitting

#### 236 | 3.1. Data

237 | We consider the case of Southern California and extract aftershock sequences  
238 | from the relocated earthquake catalog of Hauksson et al. (2012) defined over the  
239 | period 1981-2011, using the nearest-neighbor method (Zaliapin et al., 2008; used with  
240 | its standard parameters originally calibrated for Southern California, considering only  
241 | the first aftershock generation). Only events with magnitudes greater than  $m_0 = 2.0$  are  
242 | considered (a conservative estimate following results of Tormann et al. (2014);  
243 | saturation effects immediately after the mainshock are negligible when considering  
244 | entire aftershock sequences; Helmstetter et al., 2005).

245

#### 246 | 3.2. Aftershock spatial density distribution

247 | Figure 5a represents the spatial linear density distribution of aftershocks  $\rho(r)$   
248 | for the four largest strike-slip mainshocks in Southern California: 1987  $M=6.6$   
249 | Superstition Hills, 1992  $M=7.3$  Landers, 1999  $M=7.1$  Hector Mine, and 2010  $M=7.2$   
250 | El Mayor. The distance between mainshock and aftershocks is calculated as  
251 |  $r = \sqrt{(x - x_0)^2 + (y - y_0)^2}$  with  $(x, y)$  the aftershock coordinates and  $(x_0, y_0)$  the  
252 | coordinates of the nearest point to the mainshock fault rupture (as depicted in Figure  
253 | 2c). The dashed black lines shown in Figure 5a are visual guides to  $q = 1.96$ , showing  
254 | that the SSP is compatible with real aftershock observations.

255 | Comparing Figure 5a to Figure 4d suggests that  $r_*$  can be roughly estimated  
256 | from the spatial linear density plot, being the maximum distance  $r$  at which the

Arnaud Mignan 22.2.2018 16:02

Deleted: ) (

Arnaud Mignan 22.2.2018 16:02

Deleted: (

Arnaud Mignan 22.2.2018 16:02

Deleted: )

260 plateau ends, here leading to  $r_* \approx 1$  km. This parameter is constant for different large  
 261  $M$  values since both  $w_0$  and  $\Delta\sigma_0$  are constant while  $\Delta\sigma_*$  is also *a priori* a constant. We  
 262 can then estimate the ratio  $\Delta\sigma_*/\Delta\sigma_0$  from Eq. (7). However the result is ambiguous  
 263 due to uncertainties on the width  $w_0$ . For  $w_0 = \{5, 10, 15\}$  km, we get  $\Delta\sigma_*/\Delta\sigma_0 = \{-$   
 264  $0.54, -1.01, -1.38\}$ .

265 As for the plateau value  $\rho(r < r_*)$ , it provides an estimate of the aftershock  
 266 activation density  $\delta_+$  with

$$267 \quad \delta_+ = \frac{\rho(M, r < r_*)}{\exp[\ln(10)(M-4)]} \quad (14)$$

268 a volumetric density, i.e. the linear density  $\rho$  normalized by the mainshock rupture  
 269 area (Eq. 4). Due to the fluctuations in  $\rho(r < r_*)$ ,  $\delta_+$  will be estimated from the  
 270 productivity law instead (see section 3.3) and  $\rho(r < r_*)$  then estimated from Eq. (14)  
 271 (horizontal dashed colored lines), as detailed below.

272 It should be noted that we consider only the first-generation aftershocks to  
 273 avoid  $\rho$  heterogeneities from secondary aftershock clusters occurring off-fault. An  
 274 example of such heterogeneity/anisotropy is illustrated by the Landers-Big Bear case  
 275 (Fig. 2c; dotted colored curve on Fig. 5a). Those cases are not systematic and  
 276 therefore not considered in the aftershock productivity law. However they are also  
 277 due to static stress changes (e.g., King et al., 1994) with the anisotropic effects  
 278 explainable by Solid Seismicity through the concept of “historical ghost static stress  
 279 field” (Mignan, 2016a).

280

### 281 3.3. Aftershock productivity law

282 The observed number  $n$  of aftershocks of magnitude  $m \geq m_0$  produced by a  
 283 mainshock of magnitude  $M$  (for a total of  $N$  mainshocks) in Southern California is

284 shown in Figures 5b (for large  $M \geq 6$ ) and 6a (for the full range  $M \geq m_0$ ). We fit Eq.

285 (1) to the data using the MLE method with the log-likelihood function

$$286 \quad LL(\theta; X = \{n_i; i = 1, \dots, N\}) = \sum_{i=1}^N [n_i \ln[K_i(\theta)] - K_i(\theta) - \ln(n_i!)] \quad (15)$$

287 for a Poisson process, representing the stochasticity of the count  $K$  of aftershocks

288 produced by a mainshock at any given time. Inserting Eq. (1) in Eq. (15) yields

$$289 \quad LL(\theta = \{K_0, \alpha\}; X) = \ln(K_0) \sum_{i=1}^N n_i + \alpha \sum_{i=1}^N [n_i(M_i - m_0)] - K_0 \sum_{i=1}^N \exp[\alpha(M_i - m_0)] - \sum_{i=1}^N \ln(n_i!) \quad (16)$$

291 (note that the last term can be set to 0 during  $LL$  maximization). For Southern

292 California, we obtain  $\alpha_{MLE} = 2.32$  (1.01 in  $\log_{10}$  scale) and  $K_0 = 0.025$  when

293 considering large  $M \geq 6$  mainshocks only to avoid the issues of scaling break and data

294 dispersion at lower magnitudes. This result, represented by the black solid line on

295 Figure 5b, is in agreement with previous studies in the same region (e.g., Helmstetter,

296 2003; Helmstetter et al., 2005; Zaliapin and Ben-Zion, 2013; Seif et al., 2017) and

297 with  $\alpha = \ln(10) \approx 2.30$  predicted for large mainshocks in Solid Seismicity (Eq. 12).

298 Moreover we find a bulk  $\beta_{MLE} = 2.34$  (1.02 in  $\log_{10}$  scale) (Aki, 1965), in agreement

299 with  $\alpha \equiv \beta$ .

300 Let us now rewrite the Solid Seismicity aftershock productivity law (Eq. 12)

301 by only considering the large  $M$  case and injecting  $r_* = Fw_0$  (by combining Eqs. 7-8).

302 We get

$$303 \quad K(M > M_{break}) = \delta_+ \{2r_* \exp[\ln(10)(M - 4)] + \pi r_*^2 w_0\} \quad (17)$$

304 The role of  $w_0$  is illustrated in Figure 5b for different values (dashed and dotted

305 curves) and shown to be insignificant for large  $M$  values. Therefore Eq. (17) can be

306 approximated to

$$307 \quad K(M > M_{break}) \approx 2\delta_+ r_* \exp[\ln(10)(M - 4)] \quad (18)$$

308 By analogy with Eq. (1), we get



309  $\delta_+ = \frac{K_0 \exp[\ln(10)(4-m_0)]}{2r_*}$  (19)

310 With  $r_* \approx 1$  km estimated from  $\rho(r)$  (section 3.2) and  $K_0 = 0.025$ , we obtain  $\delta_+ = 1.23$   
 311 events/km<sup>3</sup> for  $m_0 = 2$ . We then get back the plateau  $\rho(r < r_*)$  for different  $M$  values  
 312 from Eq. (14), as shown in Figure 5a (horizontal dashed colored lines). Although  
 313 based on limited data, this result suggests that the activation parameter  $\delta_+$  is constant  
 314 (at least for large  $M$ ) in Southern California. Note that if  $\rho(r < r_*)$  was well  
 315 constrained, it could have been estimated jointly with  $r_*$  from Figure 5a to predict the  
 316 aftershock productivity law of Figure 5b without further fitting required (hence  
 317 removing  $K_0$  from the equation,  $K_0$  having no physical meaning in Solid Seismicity).

318

319 **4. Role of aftershock selection on productivity scaling-break**

320 We tested the following piecewise model to identify any break in scaling at  
 321 smaller  $M$ , as predicted by Eq. (12):

322 
$$K(M) = \begin{cases} K_0 \frac{\exp[\ln(10)(M_{break}-m_0)]}{\exp[\frac{3}{2}\ln(10)(M_{break}-m_0)]} \exp\left[\frac{3}{2}\ln(10)(M-m_0)\right] & , M \leq M_{break} \\ K_0 \exp[\ln(10)(M-m_0)] & , M > M_{break} \end{cases}$$

323 (20)

324 but with the best MLE result obtained for  $M_{break} = m_0$ , suggesting no break in scaling  
 325 in the aftershock productivity data, as observed in Figure 6a. Final parameter  
 326 estimates are  $\alpha_{MLE} = 1.95$  (0.85 in log<sub>10</sub> scale) and  $K_0 = 0.141$  for the full mainshock  
 327 magnitude range  $M \geq m_0$  (dotted line), subject to high scattering at low  $M$  values.

328 We now identify whether the lack of break in scaling in aftershock  
 329 productivity observed in earthquake catalogues could be an artefact related to the  
 330 aftershock selection method. We run Epidemic-Type Aftershock Sequence (ETAS)  
 331 simulations (Ogata, 1988; Ogata and Zhuang, 2006), with the seismicity rate

$$\begin{cases}
\lambda(t, x, y) = \mu(t, x, y) + \sum_{i:t_j < t} K(M_i) f(t - t_i) g(x - x_i, y - y_i | M_i) \\
f(t) = c^{p-1} (p-1) (t+c)^{-p} \\
g(x, y | M) = \frac{1}{\pi} (d e^{\gamma(M-m_0)})^{q-1} (x^2 + y^2 + d e^{\gamma(M-m_0)})^{-q} (q-1)
\end{cases} \quad (21)$$

333 Aftershock sequences are defined by power laws, both in time and space (for an  
334 alternative temporal function, see Mignan (2015; 2016b); the spatial power-law  
335 distribution is in agreement with Solid Seismicity in the case of a heterogeneous static  
336 stress field – see section 2.2).  $\mu$  is the Southern California background seismicity, as  
337 defined by the nearest-neighbor method (with same  $t, x, y$  and  $m$ ). We fix the ETAS  
338 parameters to  $\theta = \{c = 0.011 \text{ day}, p = 1.08, d = 0.0019 \text{ km}^2, q = 1.47, \gamma = 2.01, \beta =$   
339  $2.29, K_0 = 0.08\}$ , following the fitting results of Seif et al. (2017) for the Southern  
340 California relocated catalog and  $m_0 = 2$  (see their Table 1). However, we define the  
341 productivity function  $K(M)$  from Eq. (20) with  $M_{break} = 5$ . Examples of ETAS  
342 simulations are shown in Figure 6b for comparison with the observed Southern  
343 California time series. Figure 6c allows us to verify that the simulated aftershock  
344 productivity is kinked at  $M_{break}$ , as defined by Eq. (20).

345 We then select aftershocks from the ETAS simulations with the nearest-  
346 neighbor method. Figure 4d represents the estimated aftershock productivity, which  
347 has lost the break in scaling originally implemented in the simulations (with an  
348 underestimated  $\alpha_{MLE} = 2.07$  as observed in the real case for  $M \geq m_0$ ). Note that a  
349 similar result is obtained when using a windowing method (Gardner and Knopoff,  
350 1974). This demonstrates that the theoretical break in scaling predicted in the  
351 aftershock productivity law can be lost in observations due to an aftershock selection  
352 bias, all declustering techniques assuming continuity over the entire magnitude range.  
353 While such a bias is possible, it yet does not prove that the break in scaling exists. The  
354 fact that a similar break in scaling was obtained in independent Coulomb stress  
355 simulations (Hainzl et al., 2010) however provides high confidence in our results.

356 One other possible explanation for lack of scaling break is that our  
357 demonstration assumes moment magnitudes while the Southern California catalogue  
358 is in local magnitudes. Deichmann (2017) demonstrated that while  $M_L \propto M_w$  at large  
359  $M$ ,  $M_L \propto 1.5M_w$  at smaller  $M$  values. This could in theory cancel the kink in real data.  
360 However the scaling break predicted by Deichmann (2017) occurs at several  
361 magnitude units below the geometric scaling break expected by Solid Seismicity,  
362 invalidating this second option for mid-range magnitudes  $M$ .

363

## 364 5. Conclusions

365 In the present study, a closed-form expression defined from geometric and  
366 static stress parameters was proposed (Eq. 12) to explain the empirical Utsu  
367 aftershock productivity law (Eq. 1). This demonstration is similar to the previous ones  
368 made by the author to explain precursory accelerating seismicity and induced  
369 seismicity (Mignan, 2012; 2016b). In all these demonstrations, the main physical  
370 parameters remain the same, i.e. the activation density  $\delta_+$  (also  $\delta_-$  and  $\delta_0$ ), the  
371 background stress amplitude range  $\Delta\sigma_*$ , and the solid envelope  $r_*$  which describes the  
372 geometry of the “seismicity solid” (Fig. 3a-b). Further studies will be needed to  
373 evaluate whether the  $\delta_+$  and  $\Delta\sigma_*$  parameters are universal or region-specific and if the  
374 same values apply to different types of seismicity at a same location.

375 Although the Solid Seismicity Postulate (SSP) (Eq. 5) remains to be proven, it  
376 is so far a rather convenient and pragmatic assumption to determine the physical  
377 parameters that play a first-order role in the behavior of seismicity. The similarity of  
378 the SSP-simulated and observed values of the power-law exponent  $q$  of the aftershock  
379 spatial density distribution shows that the SSP is consistent with large aftershock  
380 observations once uniform noise is added to the stress field (Figs. 4d-5a). The impact

Arnaud Mignan 22.2.2018 12:09

Deleted: physical

Arnaud Mignan 22.2.2018 14:58

Deleted: , combined

Arnaud Mignan 22.2.2018 15:00

Deleted: suggests that most empirical laws observed in seismicity populations can be explained by simple geometric operations on a permanent static stress field.

Arnaud Mignan 22.2.2018 15:24

Deleted: suggests

Arnaud Mignan 22.2.2018 10:22

Deleted: a proper approach

389 | of other types of noise on  $q$  has yet to be investigated. The SSP is also complementary  
390 | to the more common simulations of static stress loading (King and Bowman, 2003)  
391 | and static stress triggering (Hainzl et al., 2010).

Arnaud Mignan 22.2.2018 16:14

Deleted: It

392 | Analytic geometry, providing both a visual representation and an analytical  
393 | expression of the problem at hand (Fig. 3), represents a new approach to try to better  
394 | understand the behavior of seismicity. Its current limitation in the case of aftershock  
395 | analysis consists in assuming that the static stress field is radial and described by Eq.  
396 | (6) (e.g., Dieterich, 1994), which is likely only valid for mainshocks relieving most of  
397 | the regional stresses and with aftershocks occurring on optimally oriented faults (King  
398 | et al., 1994). More complex, second-order, stress behaviors might explain part of the  
399 | scattering observed around Eq. (1) (Fig. 6a), such as overpressure due to trapped high-  
400 | pressure gas for example (Miller et al., 2004 – see also Mignan (2016a) for an  
401 | overpressure field due to fluid injection). Other  $\sigma(r)$  formulations could be tested in  
402 | the future, the only constraint on generating so-called seismicity solids being the use  
403 | of the postulated static stress step function of Eq. (5) (i.e., the Solid Seismicity  
404 | Postulate, SSP).

Arnaud Mignan 22.2.2018 16:14

Deleted: better

405 | Finally, the disappearance of the predicted scaling break in the aftershock  
406 | productivity law once declustering is applied (Fig. 6) indicates that more work is  
407 | required in that domain. Only a declustering technique that does not dictate a constant  
408 | scaling at all  $M$  will be able to identify rather a scaling break really exists or not.

409

410 | *Acknowledgments:* I thank N. Wetzler and two anonymous reviewers, as well as  
411 | editor Ilya Zaliapin, for their valuable comments.

412

413 | **References**

416 Abercrombie, R. and Leary, P.: Source parameters of small earthquakes recorded at  
417 2.5 km depth, Cajon Pass, Southern California: Implications for earthquake  
418 scaling, *Geophys. Res. Lett.*, 20, 1511-1514, 1993.

419 Aki, K.: Maximum Likelihood Estimate of  $b$  in the Formula  $\log N = a - bM$  and its  
420 Confidence Limits, *Bull. Earthq. Res. Instit.*, 43, 237-239, 1965.

421 Båth, M.: Lateral inhomogeneities of the upper mantle, *Tectonophysics*, 2, 483-514,  
422 1965.

423 Clauset, A., Shalizi, C. R. and Newman, M. E. J.: Power-Law Distributions in  
424 Empirical Data, *SIAM Review*, 51, 661-703, doi: 10.1137/070710111, 2009.

425 Deichmann, N.: Theoretical Basis for the Observed Break in  $M_L/M_w$  Scaling between  
426 Small and Large Earthquakes, *Bull. Seismol. Soc. Am.*, 107, doi:  
427 10.1785/0120160318, 2017.

428 Dieterich, J.: A constitutive law for rate of earthquake production and its application  
429 to earthquake clustering, *J. Geophys. Res.*, 99, 2601-2618, 1994.

430 Fan, W. and Shearer, P. M.: Local near instantaneously dynamically triggered  
431 aftershocks of large earthquakes, *Science*, 353, 1133-1136, 2016.

432 Felzer, K. R. and Brodsky, E. E.: Decay of aftershock density with distance indicates  
433 triggering by dynamic stress, *Nature*, 441, 735-738, doi: 10.1038/nature04799,  
434 2006.

435 Gardner, J. K. and Knopoff, L.: Is the sequence of earthquakes in Southern California,  
436 with aftershocks removed, Poissonian?, *Bull. Seismol. Soc. Am.*, 64, 1363-1367,  
437 1974.

438 Gu, C., Schumann, A. Y., Baisesi, M. and Davidsen, J.: Triggering cascades and  
439 statistical properties of aftershocks, *J. Geophys. Res. Solid Earth*, 118, 4278-4295,  
440 doi: 10.1002/jgrb.50306, 2013.

441 Gutenberg, B. and Richter, C. F.: Frequency of earthquakes in California, Bull.  
442 Seismol. Soc. Am., 34, 185-188, 1944.

443 Hainzl, S., Brietzke, G. B. and Zöller, G.: Quantitative earthquake forecasts resulting  
444 from static stress triggering, J. Geophys. Res., 115, B11311, doi:  
445 10.1029/2010JB007473, 2010.

446 Hauksson, E., Yang, W. and Shearer, P. M.: Waveform Relocated Earthquake Catalog  
447 for Southern California (1981 to June 2011), Bull. Seismol. Soc. Am., 102, 2239-  
448 2244, doi: 10.1785/0120120010, 2012.

449 Helmstetter, A.: Is Earthquake Triggering Driven by Small Earthquakes?, Phys. Rev.  
450 Lett., 91, doi: 10.1102/PhysRevLett.91.058501, 2003.

451 Helmstetter, A., Kagan, Y. Y. and Jackson, D. D. : Importance of small earthquakes  
452 for stress transfers and earthquake triggering, J. Geophys. Res., 110, B05S08, doi:  
453 10.1029/2004JB003286, 2005.

454 Kanamori, H. and Anderson, D. L.: Theoretical basis of some empirical relations in  
455 seismology, Bull. Seismol. Soc. Am., 65, 1073-1095, 1975.

456 King, G. C. P., Stein, R. S. and Lin, J.: Static Stress Changes and the Triggering of  
457 Earthquakes, Bull. Seismol. Soc. Am., 84, 935-953, 1994.

458 King, G. C. P. and Bowman, D. D.: The evolution of regional seismicity between  
459 large earthquakes, J. Geophys. Res., 108, 2096, doi: 10.1029/2001JB000783, 2003.

460 Lin, J. and Stein, R. S.: Stress triggering in thrust and subduction earthquakes, and  
461 stress interaction between the southern San Andreas and nearby thrust and strike-  
462 slip faults, J. Geophys. Res., 109, B02303, doi: 10.1029/2003JB002607, 2004.

463 Lippiello, E., de Arcangelis, J. and Godano, C.: Role of Static Stress Diffusion in the  
464 Spatiotemporal Organization of Aftershocks, Phys. Rev. Lett., 103, 038501, doi:  
465 10.1103/PhysRevLett.103.038501, 2009.

466 Marsan, D. and Lengliné, O.: A new estimation of the decay of aftershock density  
467 with distance to the mainshock, *J. Geophys. Res.*, 115, B09302, doi:  
468 10.1029/2009JB007119, 2010.

469 Miller, S. A., Collettini, C., Chiaraluce, L., Cocco, M., Barchi, M. and Kaus, B. J. P.:  
470 Aftershocks driven by a high-pressure CO<sub>2</sub> source at depth, *Nature*, 427, 724-727  
471 Mignan, A., King, G. C. P. and Bowman, D.: A mathematical formulation of  
472 accelerating moment release based on the stress accumulation model, *J. Geophys.*  
473 *Res.*, 112, B07308, doi: 10.1029/2006JB004671, 2007.

474 Mignan, A.: Non-Critical Precursory Accelerating Seismicity Theory (NC PAST) and  
475 limits of the power-law fit methodology, *Tectonophysics*, 452, 42-50, doi:  
476 10.1016/j.tecto.2008.02.010, 2008.

477 Mignan, A.: Retrospective on the Accelerating Seismic Release (ASR) hypothesis:  
478 Controversy and new horizons, *Tectonophysics*, 505, 1-16, doi:  
479 10.1016/j.tecto.2011.03.010, 2011.

480 Mignan, A.: Seismicity precursors to large earthquakes unified in a stress  
481 accumulation framework, *Geophys. Res. Lett.*, 39, L21308, doi:  
482 10.1029/2012GL053946, 2012.

483 Mignan, A.: Modeling aftershocks as a stretched exponential relaxation, *Geophys.*  
484 *Res. Lett.*, 42, 9726-9732, doi: 10.1002/2015GL066232, 2015.

485 Mignan, A.: Static behaviour of induced seismicity, *Nonlin. Processes Geophys.*, 23,  
486 107-113, doi: 10.5194/npg-23-107-2016, 2016a.

487 Mignan, A.: Reply to “Comment on ‘Revisiting the 1894 Omori Aftershock Dataset  
488 with the Stretched Exponential Function’ by A. Mignan” by S. Hainzl and A.  
489 Christophersen, *Seismol. Res. Lett.*, 87, 1134-1137, doi: 10.1785/0220160110,  
490 2016b.

491 Moradpour, J., Hainzl, S. and Davidsen, J.: Nontrivial decay of aftershock density  
492 with distance in Southern California, *J. Geophys. Res. Solid Earth*, 119, 5518-5535,  
493 doi: 10.1002/2014JB010940, 2014.

494 Ogata, Y.: Statistical Models for Earthquake Occurrences and Residual Analysis for  
495 Point Processes, *J. Am. Stat. Assoc.*, 83, 9-27, 1988.

496 Ogata, Y. and Zhuang, J.: Space-time ETAS models and an improved extension,  
497 *Tectonophysics*, 413, 13-23, doi: 10.1016/j.tecto.2005.10.016, 2006.

498 Richards-Dinger, K., Stein, R. S. and Toda, S.: Decay of aftershock density with  
499 distance does not indicate triggering by dynamic stress, *Nature*, 467, 583-586, doi:  
500 10.1038/nature09402, 2010.

501 Ross, Z. E., Hauksson, E. and Ben-Zion, Y.: Abundant off-fault seismicity and  
502 orthogonal structures in the San Jacinto fault zone, *Sci. Adv.*, 3, doi:  
503 10.1126/sciadv.1601946, 2017.

504 Seif, S., Mignan, A., Zechar, J. D., Werner, M. J. and Wiemer, S.: Estimating ETAS:  
505 The effects of truncation, missing data, and model assumptions, *J. Geophys. Res.*  
506 *Solid Earth*, 121, 449-469, doi: 10.1002/2016JB012809, 2017.

507 Shapiro, S. A. and Dinske, C.: Scaling of seismicity induced by nonlinear fluid-rock  
508 interaction, *J. Geophys. Res.*, 114, B09307, doi: 10.1029/2008JB006145, 2009.

509 Shaw, B. E. and Scholz, C. H.: Slip-length scaling in large earthquakes: Observations  
510 and theory and implications for earthquake physics, *Geophys. Res. Lett.*, 28, 2995-  
511 2998, 2001.

512 Shearer, P. M.: Space-time clustering of seismicity in California and the distance  
513 dependence of earthquake triggering, *J. Geophys. Res.*, 117, B10306, doi:  
514 10.1029/2012JB009471, 2012.



515 Toda, S., Stein, R. S., Richards-Dinger, K. and Bozkurt, S.: Forecasting the evolution  
516 of seismicity in southern California: Animations built on earthquake stress transfer,  
517 J. Geophys. Res., 110, B05S16, doi: 10.1029/2004JB003415, 2005.

518 Tormann, T., Wiemer, S. and Mignan, A.: Systematic survey of high-resolution b  
519 value imaging along Californian faults: inference on asperities, J. Geophys. Res.  
520 Solid Earth, 119, 2029-2054, doi: 10.1002/2013JB010867, 2014.

521 Utsu, T.: Aftershocks and Earthquake Statistics (1): Some Parameters Which  
522 Characterize an Aftershock Sequence and Their Interrelations, J. Faculty Sci.  
523 Hokkaido Univ. Series 7 Geophysics, 3, 129-195, 1970a.

524 Utsu, T.: Aftershocks and Earthquake Statistics (2): Further Investigation of  
525 Aftershocks and Other Earthquake Sequences Based on a New Classification of  
526 Earthquake Sequences, J. Faculty Sci. Hokkaido Univ. Series 7 Geophysics, 3,  
527 197-266, 1970b.

528 Utsu, T., Ogata, Y. and Matsu'ura, R. S.: The Centenary of the Omori Formula for a  
529 Decay Law of Aftershock Activity, J. Phys. Earth, 43, 1-33, 1995.

530 van der Elst, N. J. and Shaw, B. E.: Larger aftershocks happen farther away:  
531 Nonseparability of magnitude and spatial distributions of aftershocks, Geophys.  
532 Res. Lett., 42, 5771-5778, doi: 10.1002/2015GL064734, 2015.

533 Varnes, D. J.: Predicting Earthquakes by Analyzing Accelerating Precursory Seismic  
534 Activity, Pure Appl. Geophys., 130, 661-686, 1989.

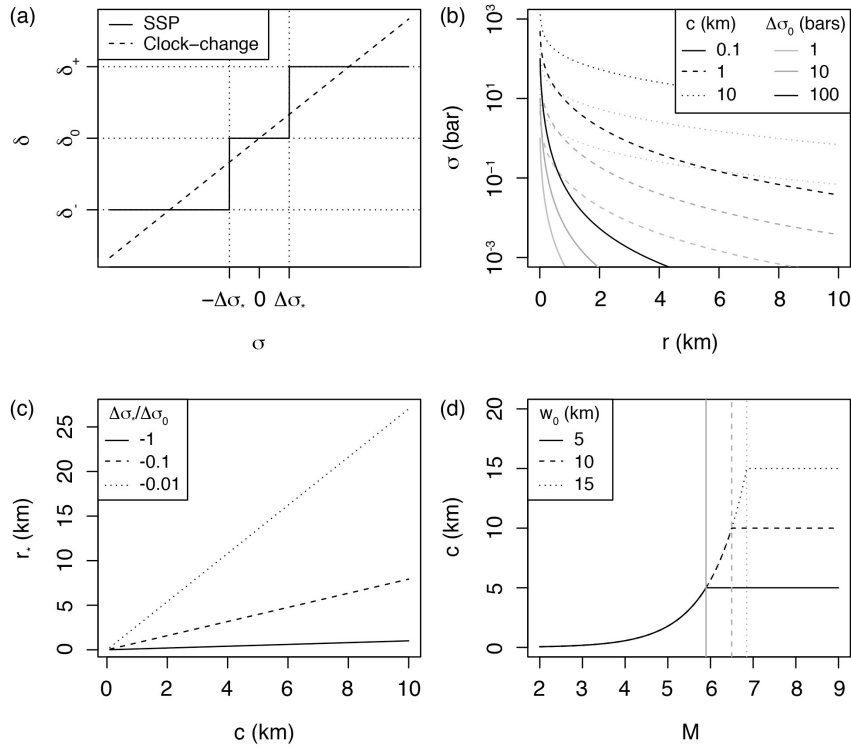
535 Yamanaka, Y. and Shimazaki, K.: Scaling Relationship between the Number of  
536 Aftershocks and the Size of the Main Shock, J. Phys. Earth, 38, 305-324, 1990.

537 Zaliapin, I., Gabrielov, A., Keilis-Borok, V. and Wong, H.: Clustering Analysis of  
538 Seismicity and Aftershock Identification, Phys. Rev. Lett., 101, 018501, doi:  
539 10.1103/PhysRevLett.101.018501, 2008.

540 Zaliapin, I. and Ben-Zion, Y.: Earthquake clusters in southern California I:  
 541 Identification and stability, *J. Geophys. Res. Solid Earth*, 118, 2847-2864, doi:  
 542 10.1002/jgrb.50179, 2013.

543

544 **Figures**



545

546 **Figure 1.** Definition of the aftershock solid envelope in a permanent static stress field:

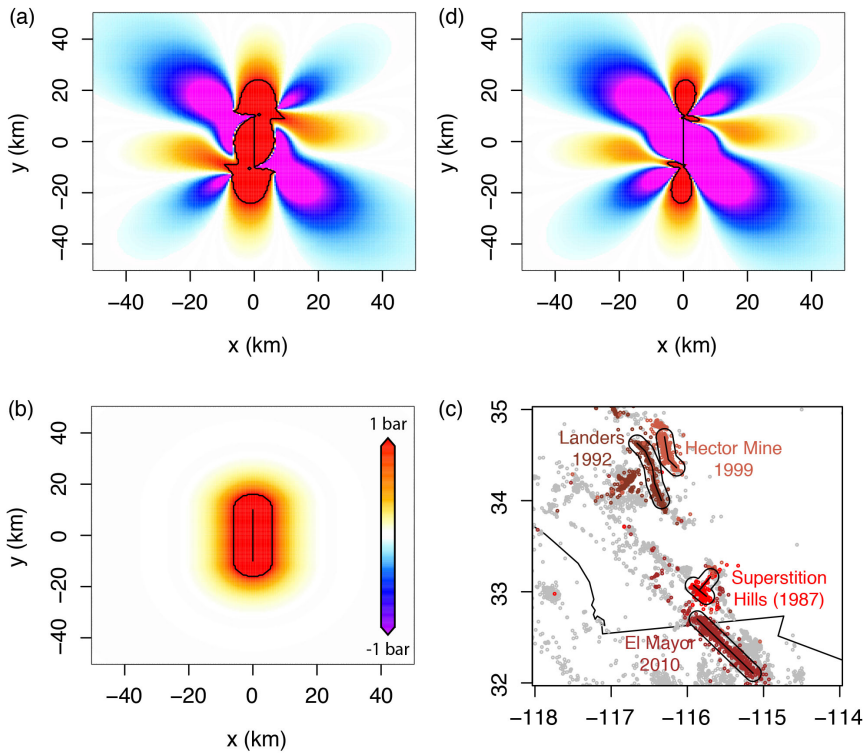
547 (a) Event density stress step-function  $\delta(\sigma)$  (Eq. 5) of the Solid Seismicity Postulate

548 (SSP) in comparison to the linear clock-change model; (b) Static stress  $\sigma$  versus

549 distance  $r$  for different effective crack radii  $c$  and rupture stress drops  $\Delta\sigma_0$  (Eq. 6); (c)

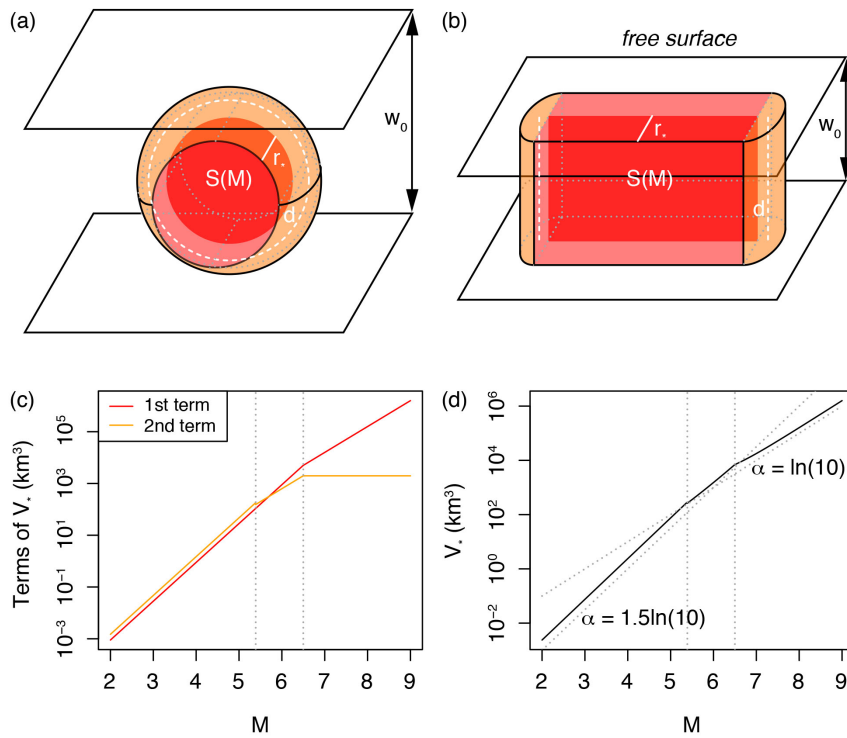
550 Linear relationship between effective crack radius  $c$  and aftershock solid envelope

551 radius  $r_*$  for different  $\Delta\sigma_*/\Delta\sigma_0$  ratios (Eq. 7); (d) Relationship between mainshock  
 552 magnitude  $M$  and effective crack radius  $c$  for different seismogenic widths  $w_0$  (Eq. 8).  
 553



554  
 555 **Figure 2.** Possible static stress fields and inferred aftershock spatial distribution: (a)  
 556 Right-lateral Coulomb stress field for optimally oriented faults, where the mainshock  
 557 relieves all of the regional stresses  $\sigma_r = 10$  bar, with  $\Delta\sigma_0 \approx -Gs/L \approx -10$  bar ( $G =$   
 558  $3.3 \cdot 10^5$  bar the shear modulus,  $s = 0.6$  m the slip,  $L = 20$  km the fault length, and  $w =$   
 559  $10$  km the fault width); (b) Radial static stress field computed from Eq. (6) with  $\Delta\sigma_0 =$   
 560  $-10$  bar and  $c = \sqrt{(Lw)/\pi}$  for consistency with (a); (c) Aftershock distribution of the  
 561 largest strike-slip events in the Southern California relocated catalog, identified here  
 562 as all events occurring within one day of the mainshock (see Data section 3.1); (d)

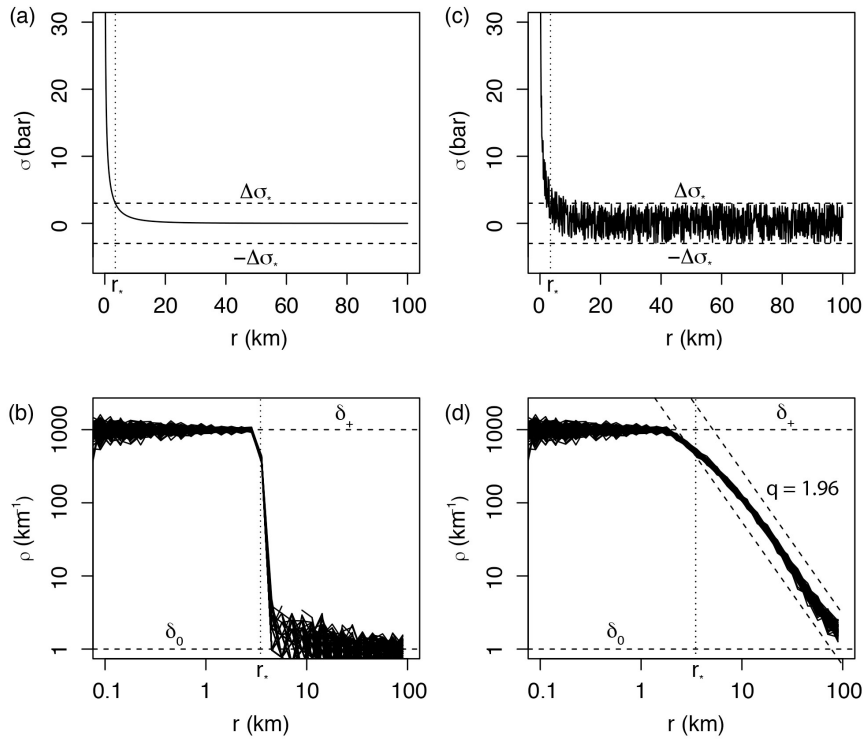
563 Right-lateral Coulomb stress field for optimally oriented faults, where the mainshock  
 564 relieves only a fraction of the regional stresses  $\sigma_r = 100$  bar with  $\Delta\sigma_0 = -10$  bar (same  
 565 rupture as in (a)) – The black contour represents 1 bar in (a), (b) and (d), and a 10 km  
 566 distance from rupture in (c). Coulomb stress fields of (a) and (d) were computed using  
 567 the Coulomb 3 software (Lin and Stein, 2004; Toda et al., 2005).  
 568



569  
 570 **Figure 3.** Geometric origin of the aftershock productivity law: (a) Sketch of the  
 571 aftershock solid for a small mainshock rupture represented by a disk; (b) Sketch of the  
 572 aftershock solid for a large mainshock rupture represented by a rectangle; (c) Relative  
 573 role of the two terms of Eq. (9), here with  $w_0 = 10$  km and  $\frac{\Delta\sigma_*}{\Delta\sigma_0} = -0.1$  (to first estimate  
 574  $c$  and  $r_*$  from Eqs. 8 and 7, respectively); (d) Aftershock productivity law (normalized  
 575 by  $\delta_+$ ) predicted by Solid Seismicity (Eq. 11). This relationship is of the same form as

576 the Utsu productivity law (Eq. 1) for large  $M$  (see text for an explanation of the lack  
 577 of break in scaling in Eq. 1 for small  $M$ ). Dotted vertical lines represent  $M$  for  
 578  $c(M) + r_*(M) = \frac{w_0}{2}$  and  $S(M) = \pi w_0^2$ , respectively.

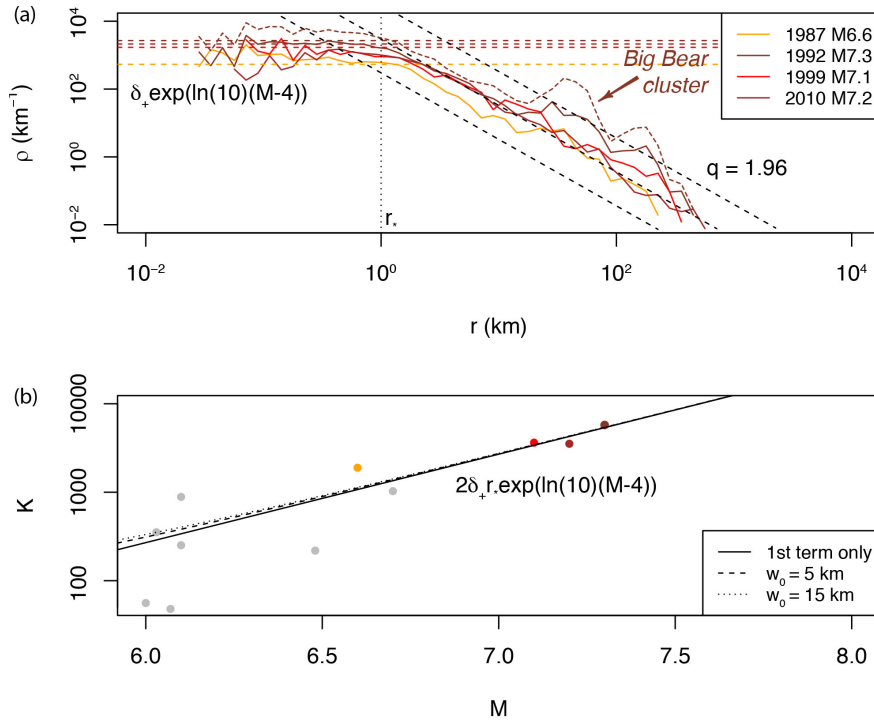
579



580

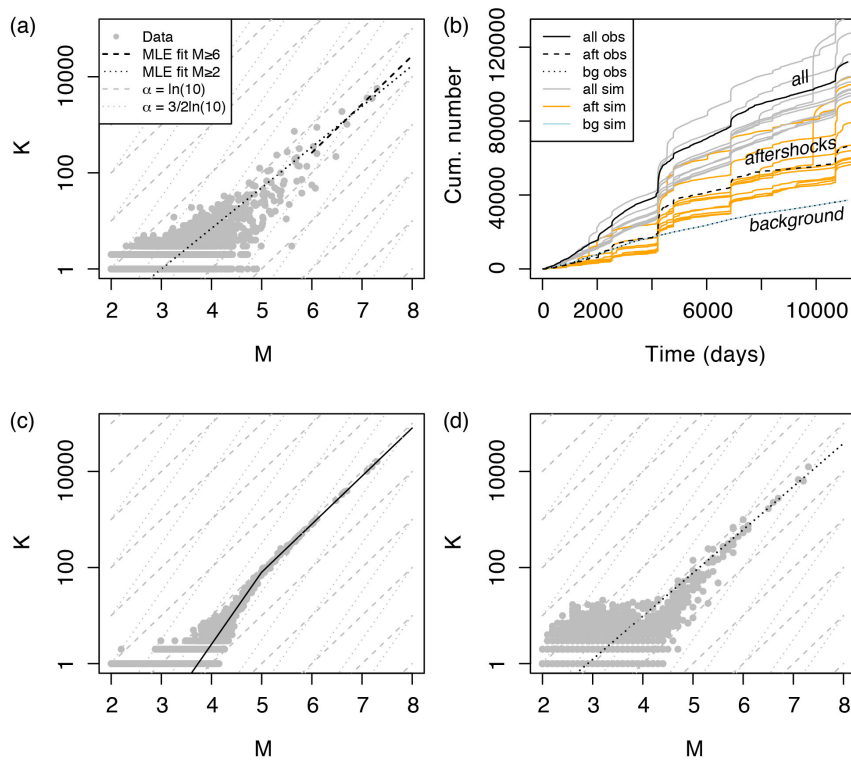
581 **Figure 4.** Spatial distribution of aftershocks following the SSP. (a) Smooth static  
 582 stress field as a function of distance  $r$  from the mainshock, with  $\Delta\sigma_0 = -10$  bar and  $c =$   
 583 10 km (Eq. 6); (b) Step-like aftershock spatial linear density  $\rho(r)$  with  $\delta_+ = 1000$   
 584 events per km,  $\delta_0 = 1$  event per km and  $\Delta\sigma_* = -0.3\Delta\sigma_0$  (*ad-hoc* ratio yielding  $r_* = 3.5$   
 585 km; Eq. (7) – event distances sampled from the  $\delta(r)$  distribution, repeated 100 times).  
 586 Such distribution is not observed in Nature; (c) Same as (a) but with random uniform  
 587 noise representative of spatial heterogeneities added to the regional stress field; (d)

588 Power-law-like aftershock spatial linear density  $\rho(r)$  with power exponent MLE  
 589 estimate  $q = 1.96$ , representative of real aftershock observations (see Fig. 5a), due to  
 590 the addition of uniform noise to the static stress field.  
 591



592  
 593 **Figure 5.** Estimating the Solid Seismicity parameters from the spatial distribution of  
 594 aftershocks: (a) Spatial linear density distribution  $\rho(r)$  of aftershocks for the four  
 595 largest strike-slip mainshocks in Southern California (with first-generation  
 596 aftershocks only; the density distribution comprising all aftershocks generated by the  
 597 Landers mainshock is represented by the dotted curve to illustrate the type of spatial  
 598 heterogeneity, such as the Big Bear cluster, not considered in the present study – see  
 599 also Fig. 2c). The Solid Seismicity parameters  $r_* = 1$  km and  $\delta_+(m_0 = 2) = 1.23$   
 600 events/km<sup>3</sup> can be retrieved from the observed plateau  $\rho(r < r_*)$ , in agreement with the

601 SSP (see Fig. 4d). Note that the spatial power-law decay at high  $r$  is similar to the one  
 602 expected by the SSP in the case of a static stress field with additive uniform noise  
 603 (expected  $q = 1.96$  represented by the dashed black lines); (b) Aftershock productivity  
 604  $K$  for  $M > 6$ . The curves represent the productivity law as defined by Solid Seismicity  
 605 (Eq. 17) for different  $w_0$  values (first term only corresponds to  $w_0 = 0$ ; Eq. 18).  
 606



607  
 608 **Figure 6.** Aftershock productivity defined as the number of aftershocks  $K(m_0 = 2)$  per  
 609 mainshock of magnitude  $M$ : (a) Observed aftershock productivity in Southern  
 610 California with aftershocks selected using the nearest-neighbor method; (b)  
 611 Seismicity time series with distinction made between background events and  
 612 aftershocks, observed (“obs”, in black) and ETAS-simulated (“sim”, colored); (c)

613 True simulated aftershock productivity with kink, defined from Eq. (20); (d)  
614 Retrieved simulated aftershock productivity with aftershocks selected using the  
615 nearest-neighbor method - Data points in (a), (c) and (d) are represented by grey dots;  
616 the model MLE fits are represented by the dashed and dotted black lines for  $M \geq 6$   
617 and  $M \geq m_0$ , respectively; dashed and dotted grey lines are visual guides to  $\alpha =$   
618  $3/2\ln(10)$  and  $\ln(10)$ , respectively.  
619